A relativistic coupled-cluster treatment of magnetic hyperfine structure of the $X^2\Pi$ and $A^2\Sigma^+$ states of OH isotopologues

D. P. Usov, Y. S. Kozhedub, N. A. V. Stolyarov, L. V. Skripnikov, N. M. Shabaev, N. and I. I. Tupitsyn Department of Physics, St. Petersburg State University,

7/9 Universitetskaya nab., 199034 St. Petersburg, Russia

Department of Chemistry, Lomonosov Moscow State University, 1/3 Leninskie gory, 119991 Moscow, Russia

National Research Centre "Kurchatov Institute" B.P. Konstantinov Petersburg

Nuclear Physics Institute, 188300 Gatchina, Leningrad district, Russia

(Dated: September 26, 2025)

Ab initio calculations of the parallel component of the magnetic dipole hyperfine structure (HFS) constant have been carried out for hydroxyl radical isotopologues $\binom{16,17}{OH(D)}$ over the internuclear distance range $R \in [0.6, 1.8]$ Å. For the ground electronic state $X^2\Pi$, the HFS functions were evaluated for contributions induced by both oxygen and hydrogen nuclei. In addition, the hydrogeninduced HFS curve was calculated for the excited $A^2\Sigma^+$ state. The quantum-chemistry study employs a four-component relativistic coupled-cluster (CC) method, including excitations up to the triple level, namely: the contribution of triple-cluster amplitudes was studied both perturbatively (CCSD(T)) and through fully iterative calculations (CCSDT). The resulting oxygen- and hydrogeninduced HFS functions represent the most accurate and reliable theoretical predictions to date exhibiting excellent agreement with semiempirical curve for hydrogen-induced HFS derived from high-resolution spectroscopic data for the lowest vibrational levels $(v \in [0,2])$ of the electronic $X^2\Pi$ state. Vibrationally averaged ab initio values are consistent with experimental values within 1% for all states considered. Furthermore, the internuclear distance range over which the HFS curves are defined has been extended beyond that of previous studies, thereby providing a robust foundation for accurate HFS treatments of higher-lying rovibrational levels of OH isotopologues within both adiabatic and non-adiabatic frameworks.

1. INTRODUCTION

The hydroxyl radical (OH) was among the first diatomic molecules to be identified in the Universe through astronomical radio spectroscopy. It exhibits a rich fine and hyperfine structure (HFS), characterized by spin—orbit coupling and Λ -doubling effects, which are essential for the unambiguous interpretation of its microwave spectra. In contrast to the fine structure, the HFS of OH depends sensitively on the nuclear spins of both oxygen and hydrogen atoms, making it a valuable probe for distinguishing between different OH isotopologues.

The OH isotopologues play a fundamental role in gas-phase chemistry and astrophysics, with relevance to interstellar and photospheric processes, atmospheric chemistry, and combustion phenomena. In atmospheric and climate studies, the OH radical is recognized as the most important oxidizing agent in the troposphere [1]. It contributes to the terrestrial nightglow [2] and plays a role in regulating the density of the ozone layer [3]. In combustion chemistry, OH is a key intermediate species, significantly influencing reaction rates, flame tempera-

tures, and the formation of pollutants [4]. In astrophysics, the interstellar OH masers are among the most common and well-studied sources of coherent cosmic emission. The HFS of OH transitions provides a powerful diagnostic tool [5] for probing magnetic fields, temperatures, masses and radiation environments in various astrophysical settings [6, 7].

For open-shell systems such as the hydroxyl radical, accurate ab initio calculations are essential to capture the complexity of electronic structure, including fine and hyperfine interactions. Previous theoretical studies have primarily employed non-relativistic methods, such as multireference configuration interaction and manybody perturbation theory (MBPT), which often provide a limited treatment of electron correlation effects. Moreover, most of these studies focus solely on the HFS parameters estimated near the equilibrium bond length or for the selected rovibrational levels, without addressing their explicit dependence on the internuclear distance R. This work addresses these limitations by employing relativistic four-component coupled-cluster (CC) theory, incorporating high-order excitations, to compute the magnetic HFS functions across a wide range of R for both the ground $X^2\Pi$ and excited $A^2\Sigma^+$ states of ($^{16,17}OH(D)$) isotopologues. The derived ab initio HFS functions enable straightforward extension of accurate HFS treatments to the higher-lying rovibrational levels of OH iso-

^{*} y.kozhedub@sbpu.ru

topologues in the framework of both conventional adiabatic approximation and advanced coupled-channel deperturbation analysis [8].

The paper is organized as follows. Section 2 provides a detailed description of the methodological approaches, computational methods and parameters used in this study. Section 3 presents the calculated HFS constants for both the ground and excited electronic states. Finally, Section 4 summarizes the main findings and conclusions of the work.

2. THEORETICAL APPROACHES AND METHODS

The calculations employ the relativistic four-component Dirac-Coulomb (DC) Hamiltonian, as implemented in the DIRAC [9] software package and its associated extensions. The DC Hamiltonian for an electronic system is given by:

$$H_{\rm DC} = \Lambda^{+} \left[\sum_{i} c \boldsymbol{\alpha}_{i} \cdot \boldsymbol{p}_{i} + \beta_{i} c^{2} + V(\boldsymbol{r}_{i}) + \sum_{i < j} \frac{1}{|\boldsymbol{r}_{i} - \boldsymbol{r}_{j}|} \right] \Lambda^{+}, \text{ical. For the ground electronic doublet state X}^{2}\Pi, \text{ calculated for several isotopologues of the hydroxyl rad-culations were performed for the HFS induced by the hydrogen nucleus (^{1}H, I = 1/2, \mu = 2.79284\mu_{N}) in the$$

where β and α are the standard 4×4 Dirac matrices, r_i and p_i denote the position and momentum operators of the *i*-th electron, $V(r_i)$ represents the total nuclear binding potential. We use atomic units unless stated otherwise. The finite nuclear size is accounted for using a Gaussian model of charge distribution. The summation goes over all electrons in the system, and Λ^+ denotes the projection operator onto the positive-energy solutions of the Dirac-Fock one-electron equation.

In magnetic dipole approximation the relativistic HFS operator is expressed as the scalar product of the electronic operator T and the nuclear magnetic moment operator μ :

$$H_{\rm hfs} = \boldsymbol{\mu} \cdot \boldsymbol{T},\tag{2}$$

where

$$T = \sum_{i} \frac{[\mathbf{r}_{i} \times \boldsymbol{\alpha}_{i}]}{r_{i}^{3}} \tag{3}$$

and

$$\mu = \frac{\mu}{I}I. \tag{4}$$

Here, μ is the nuclear magnetic moment, and I is the nuclear spin operator. We shall throughout this paper give magnetic moments in units of the nuclear magneton $\mu_{\rm N}$.

We consider the "parallel" component of the HFS constant, defined as the diagonal matrix element of $H_{\rm hfs}$

for a given electronic state ψ_n with total electronic angular momentum projection Ω onto the internuclear axis z:

$$A_{||} = \frac{\mu}{\Omega I} \left\langle \psi_n | T_z | \psi_n \right\rangle. \tag{5}$$

The diagonal matrix element in Eq. (5) can be evaluated using the finite-field approach, in which the operator T_z is added to the DC Hamiltonian $H_{\rm DC}$ with a scaling parameter λ . The expectation value is then obtained from the derivative of the total energy with respect to λ :

$$\langle \psi_n | T_z | \psi_n \rangle = \left. \frac{dE_n}{d\lambda} \right|_{\lambda=0} \approx \frac{E_n(+\Delta\lambda) - E_n(-\Delta\lambda)}{2\Delta\lambda}, \quad (6)$$

where a central finite-difference scheme is used to approximate the derivative numerically. The choice of $\Delta\lambda$ is crucial for ensuring the numerical stability and accuracy of the results. In this work, $\Delta\lambda$ is set to $1.3 \cdot 10^{-4}$ a.u..

In the present work, the HFS constants have been calculated for several isotopologues of the hydroxyl radculations were performed for the HFS induced by the hydrogen nucleus (¹H, I = 1/2, $\mu = 2.79284 \mu_{\rm N}$) in the ¹⁶OH molecule and by the oxygen nucleus (¹⁷O, I = 5/2, $\mu = -1.89379 \mu_{\rm N}$) in the ¹⁷OH molecule. For the excited $A^2\Sigma^+$ state of ¹⁶OH, the hydrogen-induced HFS was investigated. Additionally, the HFS induced by the deuterium nucleus (²D, I = 1, $\mu = 0.85743\mu_N$) was calculated for the $A^2\Sigma^+$ state of the $^{16}{\rm OD}$ molecule. The nuclear magnetic moment values were taken from [10]. All HFS constants were calculated as functions of the internuclear distance over the range $0.6 \le R \le 1.8$ Å. To enable comparison with experimental data, the obtained HFS constants were averaged over vibrational wave functions derived from semiempirical potential energy curves. For the ground state, a highly accurate semiempirical potential energy curve from Ref. [11] was used, whereas the relevant semi-empirical potential for the excited state was derived using a direct-potential-fit of the experimental A-X spectra of both OH and OD isotopologues, as reported in Ref. [12]. Although Ref. [11] provides data for the OH molecule with oxygen isotopes ¹⁶O and ¹⁸O, it does not include ¹⁷O. However, our calculations indicate that the contribution from the mass-dependent part of the potential to the ¹⁷O-induced HFS constant is negligible, less than 0.001 MHz for the lowest vibrational level, and thus below the theoretical uncertainty.

In most of the studies, the HFS constants of diatomic molecules are reported in terms of the Frosch and Foley parameters $a, b_{\rm F}, c, d$. These parameters define the matrix elements of effective operators that arise from the reduction of the four-component Dirac equation to the

two-component Pauli form [13]. The relations between the *ab initio* HFS constant $A_{||}$ and the Frosch and Foley parameters can be formulated within different Hund's coupling cases, as demonstrated, for example, in Ref. [14].

For the ground $X^2\Pi$ state of the OH molecule, which corresponds to Hund's case (a) the hyperfine constant $A_{||}$ is related to the Frosch and Foley parameters by the following expressions:

$$A_{||}\left(^{2}\Pi_{\frac{1}{2}}\right) = 2a - b_{\mathrm{F}} - \frac{2}{3}c,$$
 (7)

$$A_{||}\left(^{2}\Pi_{\frac{3}{2}}\right) = \frac{2}{3}a + \frac{1}{3}b_{\rm F} + \frac{2}{9}c.$$
 (8)

For the excited $A^2\Sigma^+$ state, which is better described by Hund's case (b), the relationship is:

$$A_{||}(^{2}\Sigma^{+}) = b_{\rm F} + \frac{2}{3}c.$$
 (9)

These expressions are employed to facilitate comparison with other experimental and theoretical results reported in terms of the Frosch and Foley parameters.

The four-component relativistic single-reference coupled-cluster method was employed, incorporating single, double, and perturbative triple excitations (CCSD(T)), as implemented in the EXP-T package [15, 16]. The hyperfine interaction operator given in Eq. (3) introduced at the coupled-cluster level, following the construction of the one-electron basis using the Dirac-Hartree-Fock method in the DIRAC program. CC calculations were performed with correlation of all 9 electrons in the OH and OD molecules, and virtual orbitals were included up to an energy cut-off of 5000 a.u.. Core-valence correlation-consistent basis sets aug-cc-pCVnZ (n=4,5) were employed, enabling extrapolation of the total energy to the complete basis set (CBS) limit using the following formula:

$$E(n) = E^{\text{CBS}} + \frac{A}{n^3}.$$
 (10)

The extrapolation formula (10) was additionally validated, and its associated error was estimated. To this end, basis sets for hydrogen and oxygen were optimized by calculations the hydrogen-induced HFS constant by the CCSD method at the equilibrium internuclear distance ($R_e = 0.96966$ Å [17]) of the $\mathrm{X^2}\Pi_{3/2}$ state of the ¹⁶OH molecule. The optimization procedure followed a strategy similar to that described in Refs [18–20]. The optimization began with the dyall.ae3z set of primitive Gaussian functions, comprising 9s2p1d functions for hydrogen and 14s8p3d1f for oxygen. Additional basis functions were incrementally added to this set, with exponents chosen to maximize the contribution of each function to the HFS constant. The final optimized basis set

included additional 6s6p4d4f1g1h functions for hydrogen and 1s4p4d2f1g1h functions for oxygen. To evaluate the residual error due to basis set incompleteness, Table 1 presents the variation of the HFS constant upon adding each type of function to the optimized basis set. The squared sum of these variations yields a total estimated uncertainty of 0.04 MHz, corresponding to less than 0.1% of the final CCSD value of 63.950 MHz at the equilibrium distance.

Table 1: Variation of hydrogen-induced HFS constant at R_e due to the inclusion of additional basis functions beyond the optimized basis set at the CCSD level.

The final CCSD(T) values for the hydrogen-induced HFS function were obtained using the optimized basis set. The associated basis set error was estimated as the difference between the values calculated with the optimized basis set and those obtained via CBS extrapolation using Eq. (10). A more detailed comparison of these results is presented in the following section.

For the oxygen-induced HFS function, the CCSD(T) values were determined through the CBS extrapolation (10) as well. The basis set error in this case was estimated as the difference between the CBS-extrapolated value and the result obtained using the aug-cc-pCV5Z basis set.

Additionally, the contribution of full triple excitations in the CC method was investigated. This contribution was determined as the difference between the CCSDT and CCSD(T) results. For the X²II state, calculations were performed using the cc-pCVQZ basis set, while for the $A^2\Sigma^+$ state, the dyall.ae4z basis set was employed. The difference between the CCSDT and CCSD(T) results was also used to estimate the uncertainty associated with the incomplete treatment of higher-order excitations.

3. RESULTS AND DISCUSSION

3.1. The ground $X^2\Pi_{1/2;3/2}$ state

1. H-induced HFS

The hydrogen-induced HFS function for the ground $\rm X^2\Pi_{3/2}$ state of $^{16}\rm OH$ molecule is represented in Figure 1. It has a strong dependence on the internuclear distance, varying from 200 MHz at 0.6 Å to -80 MHz at 1.8 Å, passing through zero around 1.4 Å. This behavior can be

attributed to a strong change in the electronic structure, in particular, the electron charge on the hydrogen atom at different internuclear distances.

A significant contribution from triple excitations in the CCSD(T) and CCSDT methods, relative to CCSD, emerges at interatomic distances exceeding 1.4 Å. In this region, the maximum coupled-cluster amplitudes reach approximately 0.1 and 0.3 for single and double excitations, respectively. Consequently, the inclusion of higher-order excitations is necessary for achieving more accurate results. At the largest available distance of 1.8 Å, the perturbative triple excitations contribute up to 80 MHz, with an additional 20 MHz arising from the inclusion of full triples.

For the HFS induced by the hydrogen nucleus, semiempirical functions are available from Ref. [11]. It is important to note that the semiempirical curve is based on experimental data for vibrational levels $v \leq 2$, corresponding to internuclear distances in the range of 0.8 to 1.3 Å, and on calculations from Ref. [21], which employed many-body perturbation theory (MBPT). These theoretical results are also shown in the figure. For internuclear distances beyond 1.4 Å, the semiempirical data rely on an extrapolation of both experimental and theoretical data. As shown in Figure 1, excellent agreement is observed between our results and the reference data in the region up to 1.4 Å. At larger distances, however, the CC curves exhibit a more pronounced decrease than predicted by the semiempirical extrapolation.

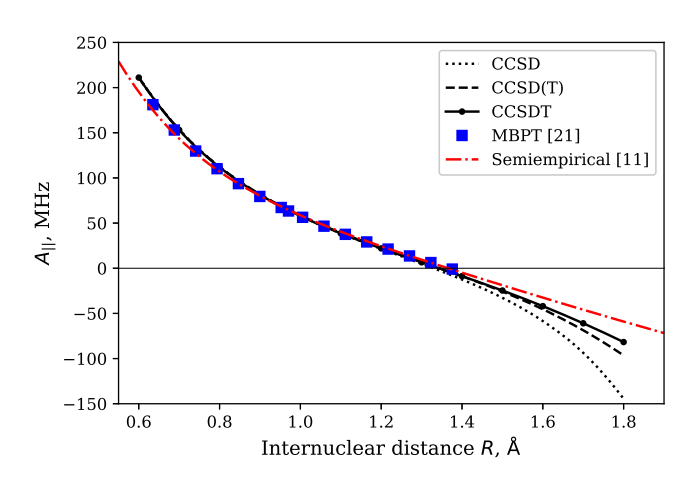


Figure 1: Calculated H-induced HFS function $A_{||}$ for $X^2\Pi_{3/2}$ state of the ¹⁶OH molecule. The semiempirical curve taken from Augustovičová and Špirko [11], as well as MBPT data from Kristiansen and Veseth [21], are also shown.

To assess the consistency between results obtained using the optimized basis set and those derived from extrapolation (10) with standard aug-cc-pCVnZ (n = 4, 5)

basis sets, a comparison of the two approaches is presented in Fig. 2. The values calculated with the optimized basis set are taken as the reference (zero baseline). The figure demonstrates that the extrapolated values closely reproduce those obtained with the optimized basis set, indicating high accuracy of the extrapolation procedure. Notably, although the basis set optimization was performed at the equilibrium bond length, the agreement persists across the entire range of internuclear distances considered.

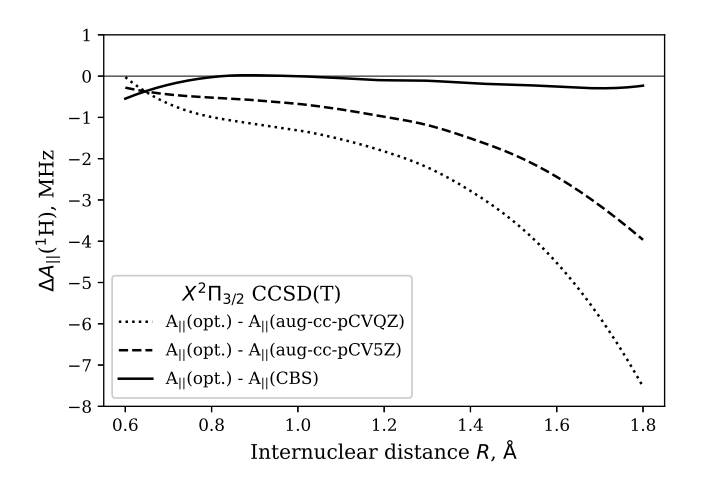


Figure 2: Basis set convergence of the H-induced HFS constant $A_{||}$ for the $X^2\Pi_{3/2}$ state. The results are based on the aug-cc-pCVnZ basis set family and are shown relative to those obtained with the optimized basis set within the CCSD(T) approximation.

For the other component of the ground-state doublet, $X^2\Pi_{1/2}$, the hydrogen-induced HFS function exhibits the behavior shown in Fig. 3. In contrast to the $X^2\Pi_{3/2}$ state, the HFS function does not change sign; instead, the curve displays a flat minimum near 1.2 Å. Beyond this minimum, the inclusion of higher-order cluster amplitudes becomes increasingly important. At an internuclear distance of 1.8 Å, the contribution from perturbative triple excitations reaches approximately 150 MHz, with an additional 60 MHz arising from the inclusion of full triples. As with the $X^2\Pi_{3/2}$ state, our final results are in good agreement with the semiempirical curve up to 1.4 Å, beyond which noticeable deviations begin to appear.

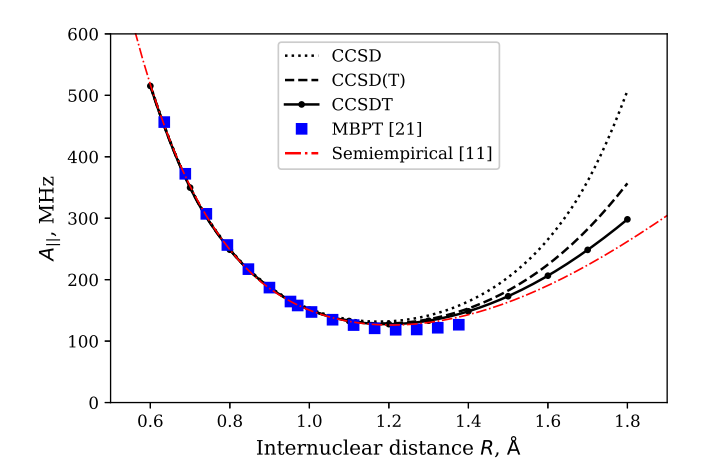


Figure 3: Calculated H-induced HFS function $A_{||}$ for $X^2\Pi_{1/2}$ state of the ¹⁶OH molecule. The semiempirical curve taken from Augustovičová and Špirko [11], as well as MBPT data from Kristiansen and Veseth [21], are also shown.

To facilitate comparison with the experimental data, the values of the hydrogen-induced HFS functions averaged over the vibrational wave functions $v \leq 2$ are given in Table 2. Since the internuclear distances relevant to these vibrational states lie within the region where the results from both the CBS extrapolation and the optimized basis set are in excellent agreement (see Fig. 2), the dominant source of uncertainty in our calculations arises from the incomplete treatment of higher-order excitations in the CC method. The contribution from triple excitations increases with vibrational quantum number. Perturbative inclusion of triple excitations via the CCSD(T) method contributes approximately 0.5 - 1.5% to the final values for the vibrational levels considered, while the inclusion of full triples using the CCSDT method adds a further 0.2 - 0.5%. The final computed values show excellent agreement with the experimental data, with deviations below 1%. Theoretical results, obtained using MBPT [21] and CASSCF/MRCI method [22], show a similar level of agreement with the experiment.

2. 17 O-induced HFS

The results for oxygen-induced HFS function in the ground state are presented in Figure 4. In contrast to the hydrogen-induced case, the curves in Figure 4 exhibit relatively weak dependence on the internuclear distance. In the non-relativistic limit this behavior can be explained by the negligible contribution of the Fermi contact term. Specifically, the unpaired electron in the π orbital does not significantly polarize the inner 1s and 2s orbitals of the oxygen atom. As a result, the HFS is pre-

dominantly determined by the spin-dipole and spin-orbit terms, which exhibit a much weaker dependence on bond length.

For the $X^2\Pi_{3/2}$ state, perturbative triple excitations contribute approximately 0.5–0.8% relative to the CCSD values up to 1.4 Å, after which the contribution increases sharply, reaching nearly 2% at 1.8 Å. In the case of the $X^2\Pi_{1/2}$ state, the contribution is around 0.1-0.2% up to 1.4 Å – but similarly rises to several percent at larger internuclear distances. Inclusion of full triple excitations via the CCSDT method, in comparison with the perturbative triples in CCSD(T), does not result in a significant change in the shape or behavior of the curves.

The values of the oxygen-induced HFS function, averaged over the vibrational wave functions, are summarized in Table 3. It is evident that the inclusion of excitations beyond CCSD does not significantly affect the results for these states. Our computed values for the lowest vibrational level show good agreement with the experimental data reported in Ref. [23, 24] for both components of the ground-state doublet. In contrast, the available theoretical results obtained using CASSCF/MRCI approach [22] exhibit noticeably larger deviations from experiment. Consequently, the reported dependence of the HFS function on internuclear distance in Ref. [22] appears unreliable, and we therefore refrain from a detailed comparative analysis of its distance dependence.

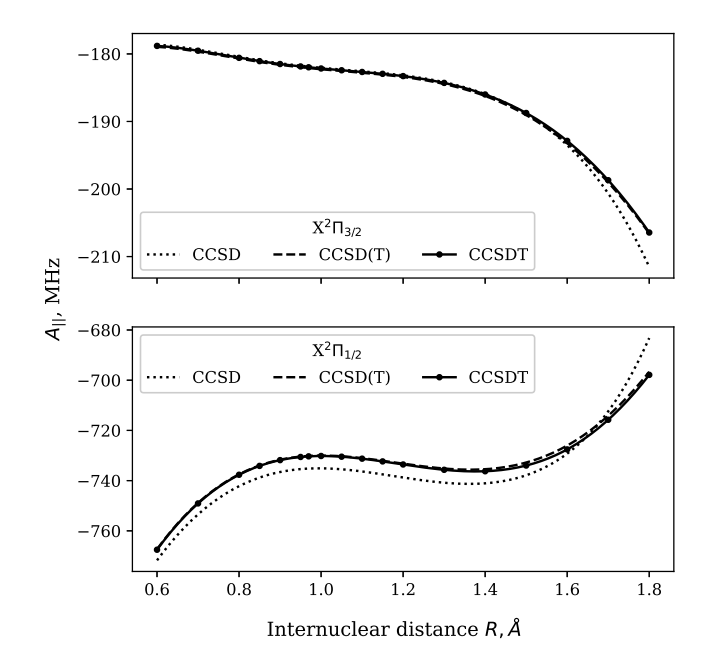


Figure 4: Calculated ¹⁷O-induced HFS function $A_{||}$ for the ${\rm X^2\Pi_{1/2}}$ and ${\rm X^2\Pi_{3/2}}$ states of the ¹⁷OH molecule.

3.2. The excited $A^2\Sigma^+$ state

The H- and D-induced HFS functions of $^{16}\mathrm{OH}$ and $^{16}\mathrm{OD}$ molecules were calculated for the first excited $\mathrm{A}^2\Sigma^+$ state. Since both nuclei involve the same electronic structure, Figure 5 shows the HFS constant curve for hydrogen only. The corresponding curve for the deuterated hydroxyl radical can be obtained by scaling the hydrogen curve by a factor $\mu_\mathrm{D}/(2\mu_\mathrm{H}) \approx 0.1535$. In the non-relativistic approach, the spin-orbit contribution vanishes, and the Fermi contact interaction becomes the dominant term determining the HFS function.

As shown in Fig. 5, the available theoretical curve obtained using third-order MBPT [21] deviates significantly from our results computed using the coupled-cluster method. To further illustrate this discrepancy, the figure also includes results from second-order Møller–Plesset perturbation theory (MP2), which exhibits similar behavior to the MBPT curve. This comparison highlights the limitations of such perturbative approaches in accurately describing the HFS in contrast to the coupled-cluster method.

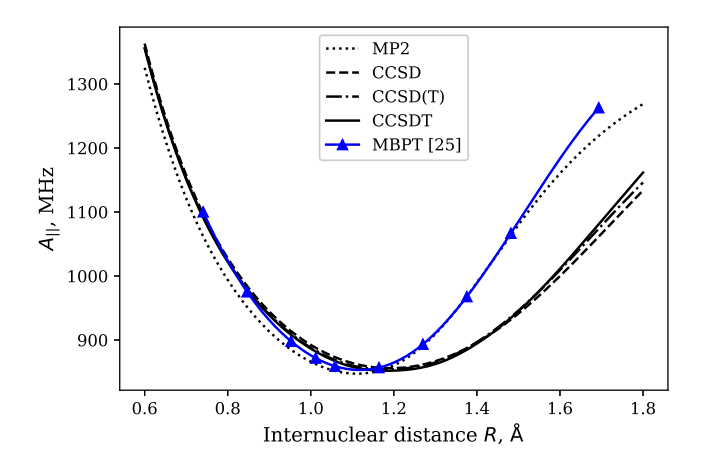


Figure 5: Calculated H-induced HFS function $A_{||}$ for the $A^2\Sigma^+$ state of the ^{16}OH molecule. Theoretical MBPT data from Kristiansen and Veseth [25] are also displayed.

Table 4 presents the HFS constants of the $^{16}\mathrm{OH}$ and $^{16}\mathrm{OD}$ molecules, averaged over the lowest vibrational states. The perturbative contribution of triple excitations within the coupled-cluster framework accounts for up to 0.5% of the final values, while the additional inclusion of full triple excitations contributes approximately 0.2% across all states considered. For the $^{16}\mathrm{OH}$ molecule, our final result for the v=0 state shows excellent agreement with all available experimental data [26–29]. However, while experimental measurements [28] report a decrease of approximately 10 MHz in the HFS constant

for the v=1 state, such a reduction is not observed in our calculations. In contrast, theoretical predictions from Ref. [25] indicate an increase in the HFS constant with vibrational excitation. For the 16 OD molecule, the vibrational dependence of the averaged HFS constant is significantly weaker, in full agreement with experimental findings [30, 31]. Other available theoretical results based on CI methods [32] exhibit larger discrepancies from experiment, particularly showing a more pronounced variation between vibrational states.

To assess the influence of relativistic effects on the HFS functions, we calculated the $A_{||}$ values using both the standard speed of light (c=137.036 a.u.) and an approximate nonrelativistic limit ($c\to\infty$), the latter modeled by increasing the standard c value by a factor of 50. Fig. 6 presents the resulting relativistic corrections to the HFS functions for all investigated states, obtained with the CCSD method and the aug-cc-pCVQZ basis set. As shown, relativistic effects are minor. For the H-induced HFS of the $X^2\Pi_{3/2}$ state and the 17 O-induced HFS of the $X^2\Pi_{1/2}$ state, the correction decreases the $A_{||}$ value, whereas in all other cases it leads to a slight increase.

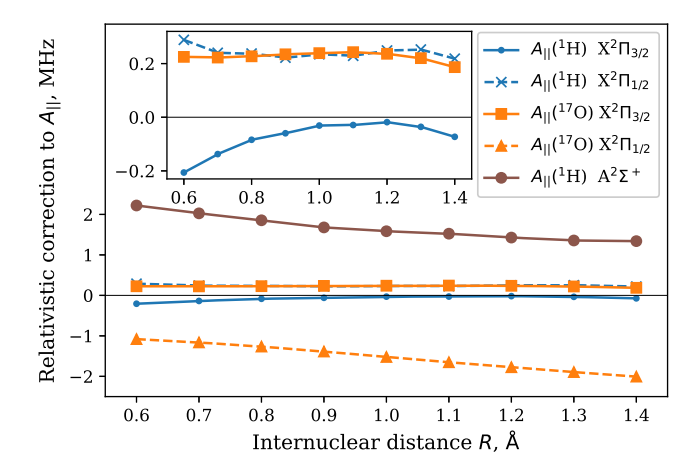


Figure 6: Relativistic correction to the HFS function $A_{||}$ for the $X^2\Pi_{1/2,3/2}$ and $A^2\Sigma^+$ states of the OH molecule for both H- and 17 O-induced hyperfine interactions.

4. CONCLUDING REMARKS

This work presents ab initio investigation of the magnetic dipole hyperfine structure (HFS) functions of the hydroxyl radical using relativistic four-component coupled-cluster theory. The study was carried out for the underlying electronic $X^2\Pi$ and $A^2\Sigma^+$ states considering HFS contributions induced by the hydrogen nucleus in both states and by the oxygen nucleus in the ground state.

The sensitivity of the results to the choice of basic sets and the level treatment of coupled-cluster excitations, was systematically investigated to ensure high accuracy and to estimate associated uncertainties. In the case of hydrogen-induced HFS, a detailed comparison was made between results obtained using a specially optimized basis set and those derived from extrapolation formulas applied to standard correlation-consistent basis sets. To evaluate the impact of higher-order excitations beyond the CCSD level, calculations were performed using both the perturbative CCSD(T) and the fully iterative CCSDT methods. The contribution of triple cluster amplitudes becomes significant at large internuclear distances R > 1.4 Å. However, for the lower vibrational levels where experimental data are available, this contribution is relatively small, ranging from 0.5% to 2%.

The HFS functions averaged over vibrational wave functions are consistent with experimental values on the order of 1% across the both states considered. The dependence of the HFS functions on the internuclear distance was systematically examined, revealing significant variation for the hydrogen-induced HFS, in contrast to the more monotonic behavior observed for the oxygen-induced HFS. Notably, the computed hydrogen-induced

HFS function for the ground state coincides with high accuracy with the available semiempirical curve within the range of distances relevant to experimental measurements.

This work demonstrates the effectiveness of relativistic quantum-chemical methods in accurately predicting HFS in molecular systems. The derived *ab initio* HFS functions provide more accurate and reliable results for the oxygen- and hydrogen-induced HFS in both the ground and excited electronic states of the OH molecule. Additionally, the range of internuclear distances for which the HFS curves are defined has been extended beyond that considered in previous studies. Consequently, the resulting functions can be readily applied for the accurate treatment of HFS in higher-lying rovibrational levels of OH isotopologues within both adiabatic and non-adiabatic frameworks.

Acknowledgments

The study was supported by the Russian Science Foundation (interdisciplinary grant No. 22-62-00004). Computations were held on the basis of the HybriLIT heterogeneous computing platform (LIT, JINR).

Table 2: $A_{||}$ constant (MHz) for the HFS, induced by the H nucleus for the $X^2\Pi$ states of the ^{16}OH molecule. The HFS constants are averaged over the vibrational wave functions.

	Ref.	$X^2\Pi_{1/2}$			$\mathrm{X}^2\Pi_{3/2}$		
		v = 0	v = 1	v = 2	v = 0	v = 1	v = 2
CCSD		160.9	161.0	162.4	61.2	55.8	50.1
CCSD(T)		159.5	159.2	160.0	61.6	56.3	50.8
CCSDT		159.2(4)	158.7(5)	159.3(7)	61.7(1)	56.5(2)	51.0(3)
MBPT	[21]	157.41	155.94	154.83	61.26	56.41	51.03
${\rm CASSCF/MRCI}$	[22]	157.23	157.26		61.71	55.59	
Expt.	[33]	158.282(14)	157.694(35)	158.081(41)	62.054(5)	56.866(12)	51.480(14)

Table 3: $A_{||}$ constant (MHz) for the HFS, induced by the ¹⁷O nucleus for the X² Π states of the ¹⁷OH molecule. The HFS constants are averaged over the vibrational wave functions.

	Ref.	$X^2\Pi_{1/2}$		$X^{2}\Pi_{3/2}$	
		v = 0	v = 1	v = 0	v = 1
CCSD		-736	-737	-181.9	-182.1
CCSD(T)		-731	-732	-182.2	-182.3
CCSDT		-731(3)	-732(3)	-182.3(6)	-182.4(6)
${\rm CASSCF/MRCI}$	[22]	-716.37	-715.62	-186.63	-187.51
Expt.	[23]	-737.4(34)		-181.8(11)	
Expt.	[24]	-729.816(138)	-182.106(46)	

	Ref.	ОН		OD			
		v = 0	v = 1	v = 0	v = 1	v = 2	v = 3
CCSD		887	888	136.2	136.3	137.0	138.4
CCSD(T)		883	884	135.6	135.6	135.7	136.5
CCSDT		881(5)	882(5)	135.3(9)	135.3(9)	135.6(9)	136.3(9)
MBPT	[25]	875.7	886.0				
CI	[32]			129.1	140.0		
Expt.	[30]			135.46(29)	135.55(29)		
Expt.	[31]			135.03(18)	135.10(26)	135.41(42)	135.89(42)
Expt.	[26]	886.7(9)					
Expt.	[27]	886.0(30)	875.8(26)				
Expt.	[28]	879.1(6)					
Expt.	[29]	879.898(73)		135.04(8)			

Table 4: $A_{||}$ constant (MHz) for the HFS, induced by the H(D) nucleus for the $A^2\Sigma^+$ state of the ^{16}OH (^{16}OD) molecule. The HFS constants are averaged over the vibrational wave functions.

- [1] D. Stone, L. K. Whalley, and D. E. Heard, Chemical Society Reviews 41, 6348 (2012).
- [2] P. Cosby and T. Slanger, Canadian journal of physics 85, 77 (2007).
- [3] J. Lelieveld, F. Dentener, W. Peters, and M. Krol, Atmospheric Chemistry and Physics 4, 2337 (2004).
- [4] T. Kathrotia, M. Fikri, M. Bozkurt, M. Hartmann, U. Riedel, and C. Schulz, Combustion and Flame 157, 1261 (2010).
- [5] S. O. M. Wright, S. K. Nugroho, M. Brogi, N. P. Gibson, E. J. W. de Mooij, I. Waldmann, J. Tennyson, H. Kawahara, M. Kuzuhara, T. Hirano, T. Kotani, Y. Kawashima, K. Masuda, J. L. Birkby, C. A. Watson, M. Tamura, K. Zwintz, H. Harakawa, T. Kudo, K. Hodapp, S. Jacobson, M. Konishi, T. Kurokawa, J. Nishikawa, M. Omiya, T. Serizawa, A. Ueda, S. Vievard, and S. N. Yurchenko, The Astronomical Journal 166, 41 (2023).
- [6] Y. Ebisawa, H. Inokuma, N. Sakai, K. M. Menten, H. Maezawa, and S. Yamamoto, The Astrophysical Journal 815, 13 (2015).
- [7] D. L. Cotten, L. Magnani, E. A. Wennerstrom, K. A. Douglas, and J. S. Onello, The Astronomical Journal 144, 163 (2012).
- [8] Q. Qu, S. N. Yurchenko, and J. Tennyson, Journal of Chemical Theory and Computation 18, 1808 (2022), https://doi.org/10.1021/acs.jctc.1c01244, PMID: 35148098.
- [9] T. Saue, R. Bast, A. S. P. Gomes, H. J. A. Jensen, L. Visscher, I. A. Aucar, R. Di Remigio, K. G. Dyall, E. Eliav, E. Fasshauer, T. Fleig, L. Halbert, E. D. Hedegård, B. Helmich-Paris, M. Iliaš, C. R. Jacob, S. Knecht, J. K. Laerdahl, M. L. Vidal, M. K. Nayak,

- M. Olejniczak, J. M. H. Olsen, M. Pernpointner, B. Senjean, A. Shee, A. Sunaga, and J. N. P. van Stralen, J. Chem. Phys. **152**, 204104 (2020).
- [10] J. E. Sansonetti and W. C. Martin, Journal of physical and chemical reference data 34, 1559 (2005).
- [11] L. D. Augustovičová and V. Špirko, Journal of Quantitative Spectroscopy and Radiative Transfer 254, 107211 (2020).
- [12] E. A. Pazyuk and A. V. Stolyarov, private communication, 2025.
- [13] R. A. Frosch and H. Foley, Physical Review 88, 1337 (1952).
- [14] M. Denis, P. A. Haase, M. C. Mooij, Y. Chamorro, P. Aggarwal, H. L. Bethlem, A. Boeschoten, A. Borschevsky, K. Esajas, Y. Hao et al., Physical Review A 105, 052811 (2022).
- [15] A. V. Oleynichenko, A. Zaitsevskii, and E. Eliav, Towards high performance relativistic electronic structure modelling: The exp-t program package, in <u>Russian</u> Supercomputing Days, pp. 375–386, Springer, 2020.
- [16] A. V. Oleynichenko, A. Zaitsevskii, and E. Eliav, Exp-t, an extensible code for fock-space relativistic coupled cluster calculations, http://www.qchem.pnpi.spb.ru/expt.
- [17] K. Huber, Molecular spectra and molecular structure: IV. Constants of diatomic molecules, Springer Science & Business Media, 2013.
- [18] N. Mosyagin, E. Eliav, A. Titov, and U. Kaldor, Journal of Physics B: Atomic, Molecular and Optical Physics **33**, 667 (2000).
- [19] M. Kaygorodov, L. Skripnikov, I. Tupitsyn, E. Eliav, Y. Kozhedub, A. Malyshev, A. Oleynichenko, V. Shabaev, A. Titov, and A. Zaitsevskii, Physical Review A 104, 012819 (2021).

- [20] M. Kaygorodov, D. Usov, E. Eliav, Y. Kozhedub, A. Malyshev, A. Oleynichenko, V. Shabaev, L. Skripnikov, A. Titov, I. Tupitsyn et al., Physical Review A 105, 062805 (2022).
- [21] P. Kristiansen and L. Veseth, The Journal of chemical physics 84, 2711 (1986).
- [22] D. P. Chong, S. R. Langhoff, and C. W. Bauschlicher Jr, The Journal of chemical physics 94, 3700 (1991).
- [23] K. R. Leopold, K. M. Evenson, E. R. Comben, and J. M. Brown, Journal of molecular spectroscopy 122, 440 (1987).
- [24] B. J. Drouin, The Journal of Physical Chemistry A 117, 10076 (2013).
- [25] P. Kristiansen and L. Veseth, The Journal of chemical physics 84, 6336 (1986).
- [26] F. Raab, T. Bergeman, D. Lieberman, and H. Metcalf,

- Physical Review A 24, 3120 (1981).
- [27] J. Ter Meulen, W. Majewski, W. L. Meerts, and A. Dymanus, Chemical Physics Letters 94, 25 (1983).
- [28] J. Ter Meulen, W. Ubachs, and A. Dumanus, Chemical physics letters 129, 533 (1986).
- [29] A. Fast, J. E. Furneaux, and S. A. Meek, Physical Review A 98, 052511 (2018).
- [30] K. German, The Journal of Chemical Physics 64, 4192 (1976).
- [31] J. Xin, I. Ionescu, D. Kuffel, and S. A. Reid, Chemical physics 291, 61 (2003).
- [32] S. Green, The Journal of Chemical Physics **58**, 4327 (1973).
- [33] J. Coxon, Canadian Journal of Physics 58, 933 (1980).